Dynamic Properties and Electrostatic Potential Surface of Neutral DNA Heteropolymers

Frederick H. Hausheer,*,†,‡ U. Chandra Singh,§ Thomas C. Palmer,∥ and Jeffrey D. Saxe⊥

Contribution from the Molecular Design Laboratory, Cancer Therapy and Research Center, 4450 Medical Drive, San Antonio, Texas 78229, Drug Development Section, Division of Medical Oncology, University of Texas Health Sciences Center, San Antonio, Texas 78229, Molecular Biology, Scripps Clinic and Research Foundation, 10666 North Torrey Pines Road, La Jolla, California 92037, North Carolina Supercomputing Center, 3021 Cornwallis Road, Research Triangle Park, North Carolina 27709, and Sterling Research Group, 9 Great Valley Parkway, Malvern, Pennsylvania 19355. *Received April 12, 1990*

Abstract: Molecular dynamics simulations of fully substituted methylphosphonate (MP) dsDNA of d[AT]5-d[AT]5 and d[GC]5-d[GC]5 were carried out by using explicit water with periodic boundaries at 300 K for 50 ps. MP substitution increased the hydrophobic behavior and neutralized the negative charge of the phosphate backbone of the dsDNA heteropolymers, resulting in a series of specific conformational and physicochemical changes in the dsDNA heteropolymers. The electrostatic potential surface of these neutral dsDNA heteropolymers was calculated by use of a 6-31G* basis set, and a difference was observed in the electrostatic potential for the two neutral DNA helices. These findings support that the role of the negative phosphate backbone is important for interactions with the solvent and counterions, and that charge neutralization of the backbone has relatively small effects upon the conformational properties of DNA.

Introduction

The role of the phosphate backbone in determining the conformational and physicochemical behavior of double-strand DNA (dsDNA) and single-strand DNA (ssDNA) is fundamentally important to understanding many biochemical and biologic processes. The consequences of rendering the negative charge of the phosphate backbone neutral with regard to the dynamic, conformational, and electrostatic properties of DNA are unknown for dsDNA molecules. The study of neutral (nonionic) phosphate substitutions and their effects on DNA structure and stability would provide useful information regarding the physicochemical role of the native phosphodiester moiety in DNA for developing DNA sequence specific compounds for biologic research, and for diagnostic and therapeutic applications. It is increasingly observed that molecular recognition interaction between DNA and a variety of molecules (e.g., drugs, proteins) is a concerted event, dependent in part upon interactions mediated by the phosphodiester backbone.

Among the most extensively studied neutral phosphate modifications are the methylphosphonates (MP) developed by Miller and Ts'o.[1,2] Methyl substitution of one of the anionic phosphoryl oxygens incorporated into DNA oligomers renders the net negative charge of the backbone neutral, resulting in profound alterations in biochemical properties of single-strand DNA molecules including increased lipid solubility, nuclease resistance, and maintenance of sequence specificity for complementary DNA or RNA sequences. Single-strand MP DNA oligomers can penetrate living cells and have been shown to inhibit mRNA translation in globin synthesis, vesicular stomatitis viral protein synthesis, and splicing of pre-mRNA resulting in inhibition of HSV replication.[1-6] The dynamic conformational behavior of synthetic MP-ssDNA oligomers has received little investigation, and studies of dsDNA molecules containing MP substitutions have not been reported. We have studied the conformational behavior of native and MP-substituted DNA oligomers incorporated into DNA triple helices by molecular dynamics and observed a variety of conformational changes along with evidence of tighter hybridization of the MP oligomers over native oligomers to DNA duplex targets.[7] Enhanced hybridization of MP-ssDNA oligomers to complementary ssDNA targets is postulated to occur as a result of decreased interstrand phosphate repulsion between the neutral MP-substituted oligomer and negative phosphate groups on the target DNA strand.[1]

We were interested in studying the dynamic and conformational behavior of neutral dsDNA heteropolymers to understand the role of the negatively charged phosphate backbone with regard to physicochemical properties of DNA. This information would be useful in designing additional chemical modifications of the phosphodiester backbone and help to formulate a rational basis to enhance the stability of DNA or RNA hybridization. Another goal of these studies was to study the electrostatic potential surface of neutral DNA heteropolymers to improve the understanding of the accessibility of the nucleobase atoms for chemical interactions and the charge distribution of the exposed DNA surface. To study the electrostatic properties of these neutral dsDNA molecules, atomic point charges were calculated for the molecular fragments database fitted to the molecular electrostatic potential by using ab initio quantum mechanical 6-31G* basis set derived charges. In addition, calculations of RNA and native phosphodiester groups for all-atom and united-atom representations were performed to uniformly update the nucleic acid database.

Methods

The MP backbone conformations, force field parameters, and partial atomic charge assignments were calculated by ab initio quantum mechanical methods using QUEST.[8] The ab initio gradient (geometry) optimization of methylphosphonate dimethyl ester (MPDE) was performed with a 3-21G* basis set. All internal degrees of freedom in the molecule were optimized with the exception of C-H bonds on the end ether methyl groups (which were treated as single parameters). The starting geometry of the MPDE molecule was built by using standard bond lengths and angles, with the dihedral angles similar to that of the DNA backbone.

† Cancer Therapy and Research Center.
‡ University of Texas Health Sciences Center.
§ Scripps Clinic and Research Foundation.
∥ North Carolina Supercomputing Center.
⊥ Sterling Research Group.

(1) Miller, P. S.; Ts'o, P. O. P. *Anti-Cancer Drug Des.* **1987**, *2*, 117-128.
(2) Miller, P. S.; Dreon, N.; Pulford, S. M.; McParland, K. B. *J. Biol. Chem.* **1980**, *255*, 9659-9665.
(3) Agris, C. H.; Blake, K. R.; Miller, P. S.; Reddy, M. P.; Ts'o, P. O. P. *Biochemistry* **1986**, *25*, 6268-6275.
(4) Blake, K. R.; Murakami, A.; Miller, P. S. *Biochemistry* **1985**, *24*, 6132-6138.
(5) Murakami, A.; Blake, K. R.; Miller, P. S. *Biochemistry* **1985**, *24*, 4041-4046.
(6) Smith, C. C.; Aurelian, L.; Reddy, M. P.; Miller, P. S.; Ts'o, P. O. P. *Proc. Natl. Acad. Sci. U.S.A.* **1986**, *23*, 2787-2791.
(7) Hausheer, F. H.; Singh, U. C. S.; Saxe, J. D.; Colvin, O. M.; Ts'o, P. O. P. *Anti-Cancer Drug Des.* **1990**, *5*, 159-167.
(8) Singh, U. C.; Kollman, P. A. J. *Comput. Chem.* **1984**, *2*, 129-145.

0002-7863/90/1512-9468$02.50/0

Table I. Charges for 1-Aminodeoxyribose

	all-atom charges		united-atom charges	
atom	6-31G*	STO-3G	6-31G*	STO-3G
O1′	−0.536	−0.368	−0.532	−0.386
C1′	0.888	0.558	0.719	0.502
C4′	0.188	0.036	0.358	0.185
C2′	−0.420	−0.307	−0.056	−0.047
C3′	0.228	0.233	0.169	0.172
N1′	−1.322	−0.869	−1.296	−0.876
O3′	−0.719	−0.508	−0.723	−0.514
C5′	0.121	0.118	0.168	−0.153
H1′	−0.012	0.009		
HNA′	0.455	0.305	0.458	0.313
HNB′	0.486	0.329	0.482	0.327
H2A′	0.142	0.081		
H2B′	0.088	0.081		
H3′	0.043	0.025		
H4′	0.065	0.056		
HO3′	0.444	0.306	0.445	0.313
O5′	−0.616	−0.404	−0.591	−0.425
H5A′	0.000	0.003		
H5B′	0.061	0.039		
HO5′	0.413	0.279	0.399	0.285
dipole				
MX	2.247	1.783	2.250	1.799
MY	−2.046	−1.619	−2.061	−1.619
MZ	0.122	0.215	0.156	0.234
Σ	0.91	0.68	1.21	0.85
rms	7.7	7.4	10.2	9.4

All-atom (with explicit aliphatic hydrogens) and united-atom (lacking explicit aliphatic hydrogens) partial atomic charges for aminodeoxyribose, 1-aminoribose, 9-methylguanosine, 9-methyladenosine, 1-methylcytosine, 1-methylthymine, 1-methyluracil, dimethyl phosphate diester, and the MPDE were derived from ab initio calculations using a 6-31G* basis set. The monopole atomic charges were fitted to the calculated molecular electrostatic potential. The final monopole charge assignments for the MPDE fragment were balanced to obtain a net neutral charge for each base, sugar, and MP diester unit in the DNA.

Computer-generated molecular models of d[AT]5-d[AT]5 and d-[GC]5-d[GC]5, (hereafter identified as AT and GC, respectively) were built using a B-DNA starting geometry.[9] Alternating (*R*)- and (*S*)-MP diastereomer substitutions were made along both backbones in each of the two DNA heteropolymers. The alternating pattern of MP diastereomers was introduced to simulate the approximate experimental yield, since the stereospecific synthesis of MPs cannot be readily controlled. The two DNA helices were surrounded by a 10-Å shell of TIP3P water molecules[10] with periodic boundary conditions. The size of the periodic box was X = 56.0 Å, Y = 42.2 Å, and Z = 40.8 Å for the AT ensemble, and X = 56.3 Å, Y = 42.2 Å, and Z = 41.2 Å for the GC ensemble. There were approximately 2570 water molecules solvating each dsDNA molecule, and the average total number of atoms in each system was 8310.

Molecular mechanics and molecular dynamics calculations using an all-atom force field were made with a fully vectorized version of AMBER (version 3.2) optimized for Cray supercomputers.[11] All molecular mechanics and dynamics calculations were performed on either a Cray X-MP/24 or Cray X-MP/14SE. The DNA atoms were initially fully constrained while the solvent molecules were energy minimized by using an 8 Å-nonbonded cutoff for 3500 cycles. The DNA and TIP3P waters were subsequently energy minimized without constraints for 2500 cycles with an 8 Å-nonbonded cutoff, followed by 200 cycles of energy minimization with SHAKE bond constraints activated.[12] Molecular dynamics at constant temperature (300 K) and pressure (1 bar = 1 atm) and with periodic boundaries were carried out with SHAKE constraints for 40 ps following an initial 10 ps of equilibration for both helical systems. A time step of 0.002 ps was used for the simulations, and the average temperature remained near 300 K (±3.6 K) throughout. There were no detectable artifacts due to inaccuracies in numerical integration for any of the simulations. Data analysis of the molecular dynamics run for the two systems was made on the final 40-ps trajectories.

Table II. Charges for 1-Aminoribose

	atom-atom charges		united-atom charges	
atom	6-31G*	STO-3G	6-31G*	STO-3G
O1′	−0.564	−0.343	−0.589	−0.413
C1′	0.767	0.373	0.842	0.537
C4′	0.300	0.100	0.364	0.197
C2′	−0.003	0.101	−0.048	0.083
C3′	0.310	0.303	0.316	0.271
N1′	−1.273	−0.828	−1.318	−0.894
O3′	−0.727	−0.520	−0.753	−0.542
C5′	0.197	0.180	0.214	0.175
HI′	0.033	0.054		
HNA′	0.456	0.312	0.467	0.325
HNB′	0.466	0.308	0.474	0.317
H2′	0.026	0.008		
O2′	−0.704	−0.546	−0.722	−0.512
H3′	0.018	0.007		
H4′	0.028	0.061		
HO3′	0.438	0.303	+0.448	0.316
O5′	−0.669	−0.463	−0.684	−0.488
H5A′	0.003	0.001		
H5B′	0.021	0.016		
HO5′	0.417	0.289	0.421	0.300
HO2′	0.466	0.324	0.469	0.329
dipole				
MX	2.020	1.723	2.051	1.749
MY	−2.184	−1.740	−2.185	−1.754
MZ	0.938	0.836	0.953	0.848
Σ	0.96	0.69	1.01	0.75
rms	7.4	6.9	7.6	7.6

Table III. Charges for 1-Methylthymine

	all-atom charges		united-atom charges	
atom	6-31G*	STO-3G	6-31G*	STO-3G
N1	−0.164	−0.233	−0.802	−0.739
C2	0.867	0.849	1.241	1.113
N3	−0.826	−0.851	−1.100	−1.012
C4	0.800	0.809	1.075	0.980
C5	−0.079	−0.176	−0.710	−0.595
C6	−0.122	0.034	0.657	0.551
O2	−0.632	−0.488	−0.688	−0.529
O4	−0.603	−0.464	−0.611	−0.472
C7	−0.439	−0.382	0.167	0.097
H7A (0.1375)	0.165	0.119		
H7B (0.1375)	0.123	0.111		
H7C (0.1375)	0.123	0.111		
C1M	−0.216	−0.251	0.305	0.236
HC1A	0.122	0.118		
HC1B	0.122	0.103		
HC1C	0.122	0.103		
HN3	0.433	0.355	0.465	0.370
H6	0.222	0.134		
dipole				
MX	1.300	−0.981	−1.252	−0.975
MY	0.000	0.000	0.000	0.000
MZ	−4.943	−3.238	−4.898	−3.175
Σ	0.63	0.58	2.41	1.23
rms	4.7	6.1	12.0	12.9

Calculation of the electrostatic potential surfaces of the two DNA heteropolymers was carried out with the time-averaged structural coordinates from the 40-ps trajectories. The electrostatic potential of the DNA at the solute–solvent interface was approximated by calculation of the potential at a distance of 1.4 Å (half the diameter of a water molecule) from the van der Waals radius of each atom using the 6-31G* point charges. The calculation of the electrostatic potential V_{esp} at spatial points F for a system of charges q_i in a medium of dielectric constant ϵ is given by

$$V_{esp} = \sum_i \frac{q_i}{\epsilon |r_i - F|}$$

The electrostatic potential surface of the DNA was rendered by using

(9) Arnott, S.; Selsing, E. *J. Mol. Biol.* **1975**, *98*, 265–269.
(10) Jorgensen, W. L.; Chandrasekkar, J.; Madura, J. D.; Impey, R. W.; Klein, M. L. *J. Chem. Phys.* **1983**, *79*, 926–935.
(11) Singh, U. C.; Weiner, P. K.; Seibel, G.; Kollman, P. A. AMBER version 3.2; 1989.
(12) Van Gunstersen, W. F.; Berendsen, H. J. C. *Mol. Phys.* **1977**, *34*, 1311–1327.

Table IV. Charges for 1-Methylcytosine

	all-atom charges		united-atom charges	
atom	6-31G*	STO-3G	6-31G*	STO-3G
N1	−0.267	−0.187	−0.703	−0.572
C2	0.980	0.859	1.033	0.939
N3	−0.931	−0.860	−0.776	−0.791
C4	1.120	0.935	0.532	0.629
C5	−0.793	−0.576	−0.178	−0.230
C6	−0.195	0.185	0.471	0.377
O2	−0.673	−0.508	−0.670	−0.518
N4	−1.125	−0.834	−0.950	−0.743
C1M	−0.179	−0.289	0.361	0.235
HN4A	0.482	0.351	0.462	0.338
HN4B	0.456	0.329	0.463	0.335
H5	0.252	0.153		
H6	0.172	0.098		
HC1A	0.086	0.116		
HC1B	0.111	0.115		
HC1C	0.111	0.115		
dipole				
MX	5.164	3.517	5.182	3.509
MY	0.000	0.000	0.000	0.000
MZ	−5.343	−4.181	−5.217	−4.056
Σ	0.64	0.56	2.41	1.64
rms	3.2	3.7	12.0	11.0

Table V. Charges for 1-Methyluracil

	all-atom charges		united-atom charges	
atom	6-31G*	STO-3G	6-31G*	STO-3G
N1	−0.112	−0.159	−0.673	−0.570
C2	0.833	0.775	0.988	0.896
N3	−0.759	−0.768	−0.753	−0.758
C4	0.909	0.834	0.480	0.572
C5	−0.606	−0.529	−0.099	−0.205
C6	0.059	0.160	0.441	0.367
O2	−0.625	−0.472	−0.643	−0.494
O4	−0.634	−0.474	−0.502	−0.394
C1M	−0.284	−0.329	0.328	0.239
H3	0.405	0.334	0.433	0.347
H5	0.234	0.146		
H6	0.187	0.098		
HC1A	0.127	0.133		
HC1B	0.133	0.126		
HC1C	0.133	0.126		
dipole				
MY	−2.209	−1.628	−2.253	−1.667
MY	0.000	0.000	0.000	0.000
MZ	−5.050	−3.264	−4.913	−3.130
Σ	0.70	0.56	2.57	1.70
rms	4.6	5.4	16.58	6.3

a molecular ray-tracing program[13] on a Silicon Graphics Iris workstation.

Results

Ab Initio Studies. The computed electrostatic charges for 1-aminodeoxyribose, 1-aminoribose, 9-methylguanosine, 9-methyladenosine, 1-methylcytosine, 1-methylthymine, 1-methyluracil, and dimethyl phosphate diester are shown in Tables I–VIII. In general, the 6-31G*-derived charges are qualitatively similar to previously calculated STO-3G charges[8] for the all-atom and united-atom molecular representations. The differences between 6-31G* and STO-3G charges can be observed in the oxygen and nitrogen atoms and their neighbors; the 6-31G* basis set uniformly assigns more negative charges to electronegative atoms and more positive charge values to their covalently attached atoms than the STO-3G basis set. The 6-31G* electrostatic potential charges have consistently higher values than the STO-3G charges, which is due to the inclusion of polarization functions on heavy atoms resulting in higher monopolar charge densities with the 6-31G* basis set.

Table VI. Charges for 9-Methyladenine

	all-atom charges		united-atom charges	
atom	6-31G*	STO-3G	6-31G*	STO-3G
NI	−0.866	−0.774	−0.907	−0.760
C2	0.627	0.661	0.764	0.571
N3	−0.796	−0.728	−0.812	−0.717
C4	0.529	0.546	0.618	0.695
C5	−0.122	−0.097	−0.216	−0.151
C6	0.909	0.769	0.926	0.813
N7	−0.585	−0.543	−0.660	−0.599
C8	0.192	0.263	0.583	0.488
N9	−0.055	−0.063	−0.460	−0.451
N6	−1.058	−0.768	−1.041	−0.793
H2	0.063	−0.032		
H8	0.143	0.062		
C1M	−0.382	−0.431	0.288	0.230
HN6A	0.462	0.335	0.456	0.335
HN6B	0.451	0.324	0.460	0.340
HCIA	0.146	0.158		
HCIB	0.170	0.159		
HC1C	0.170	0.159		
dipole				
MX	2.651	2.274	2.612	2.227
MY	0.000	0.000	0.000	0.000
MZ	0.430	0.264	0.342	0.204
Σ	0.96	0.07	1.67	1.23
rms	8.7	8.8	15.1	11.05

Table VII. Charges for 9-Methylguanine

	all-atom charges		united-atom charges	
atom	6-31G*	STO-3G	6-31G*	STO-3G
N1	−0.831	−0.729	−0.919	−0.746
C2	1.062	0.871	1.060	0.842
N3	−0.766	−0.709	−0.757	−0.702
C4	0.312	0.391	0.504	0.490
C5	−0.000	−0.060	−0.133	−0.088
C6	0.741	0.690	0.859	0.714
N7	−0.547	−0.543	−0.633	−0.575
C8	0.134	0.266	0.580	0.428
N9	0.009	0.022	−0.526	−0.360
N2	−1.120	−0.778	−1.112	−0.758
O6	−0.602	−0.458	−0.614	−0.459
H1	0.422	0.336	0.436	0.340
H8	0.153	0.046		
C9M	−0.396	−0.459	0.313	0.216
HN2A	0.481	0.339	0.474	0.333
HN2B	0.461	0.325	0.467	0.324
HC9A	0.152	0.163		
HC9B	0.166	0.164		
HC9C	0.166	0.164		
dipole				
MX	−3.485	−3.416	−3.595	−3.471
MY	0.000	0.000	0.000	0.000
MZ	7.401	5.357	7.368	5.294
Σ	0.86	0.89	1.51	1.22
rms	4.3	5.6	7.6	7.7

The results of ab initio quantum mechanical (RHF 3-21G*) optimized "*R* and *S*" MPDE diastereomer geometries compared to an X-ray crystallographic structure[14] of a thymine dinucleotide oligomer containing an (*S*)-MP diastereomer are shown in Table IX. The ab initio calculated bond lengths and angles are within experimental error ($R = 0.105$) of the X-ray structure. The absolute mean error differences for the bond lengths are 0.02 Å, and 1.2° for bond angles for the calculated vs X-ray structures of (*S*)-MP.

Molecular Dynamics Studies. The averaged helical repeat angles and number of base pairs per 360° turn show that both neutral DNA systems are unwound (fewer base pairs per turn) relative to idealized B DNA over the dynamics trajectory (Tables

(13) Palmer, T. C.; Hausheer, F. H.; Saxe, J. D. Applications of Ray-Tracing in Molecular Graphics. *J. Mol. Graphics* **1989**, *7*, 160–164.

(14) Chacko, K. K.; Lindner, K.; Saenger, W.; Miller, P. S. *Nucleic Acids Res.* **1983**, *11*, 2801–2814.

Table VIII. Charges for Dimethyl Phosphate

	all-atom charges		united-atom charges	
atom	6-31G*	STO-3G	6-31G*	STO-3G
P	2.049	1.560	2.301	0.913
OCA	−0.862	−0.509	−0.825	−0.409
OCB	−0.862	−0.508	−0.821	−0.410
CA	−0.092	0.032	0.282	0.108
CB	−0.092	0.037	0.283	0.110
OPA	−0.996	−0.846	−1.109	−0.655
OPB	−0.997	−0.848	−1.111	−0.657
H	0.118	0.003		
H	0.173	0.025		
H	0.135	0.014		
H	0.118	0.002		
H	0.173	0.023		
H	0.135	0.015		
Σ	1.44	1.17	1.55	1.17
rms	1.6	1.2	1.7	1.3

Table IX. Comparison of ab Initio Quantum Mechanical Calculated (RHF 3-21G*) Geometries of (*S*)- and (*R*)-Methylphosphonate Dimethyl Ester to an X-ray Crystallographic Structure Containing an (*S*)-Methylphosphonate Diastereomer[14]

	(*S*)-MP	(*R*)-MP	crystal [(*S*)-MP)]
bond, Å			
C1–O1	1.45	1.46	1.47
C2–O2	1.46	1.46	1.47
P–O1	1.58	1.57	1.57
P–O2	1.59	1.59	1.57
P–CP	1.78	1.78	1.80
P–OP	1.46	1.46	1.49
angle, deg			
C1–O1–P	127.2	123.1	123, 119
C2–O1–P	123.6	124.0	123, 119
O1–P–CP	105.3	101.7	105, 119
O2–P–CP	102.2	105.7	105, 119
O1-P-OP	113.3	116.2	113, 116
O2-P-OP	113.8	112.2	113, 116
O1-P-O2	103.9	102.4	104
CP-P-OP	116.9	116.9	116

Table X. Helical Twist Angles[a] (rms)

	AT		GC
T2-A19	25.3 (11.1)	C2-G19	26.8 (10.0)
A3-T18	45.8 (25.2)	G3-C18	30.2 (6.4)
T4-A17	14.9 (8.1)	C4-G17	17.0 (5.7)
A5-T16	26.0 (11.0)	G5-C16	23.7 (6.5)
T6-A15	31.7 (8.6)	G6-G15	11.1 (5.1)
A7-T14	48.2 (8.0)	G7-C14	20.2 (10.1)
T8-A13	18.9 (7.0)	C8-G13	25.9 (5.7)
A9-T12	27.6 (8.8)	G9-C12	33.7 (8.9)
av	29.8 (10.9)		23.6 (7.3)

[a] In degrees.

Table XI. Helical Repeat Angles[a] (rms)

	AT		GC
T2-A19	47.9 (7.4)	C2-G19	38.2 (10.0)
A3-T18	43.7 (4.6)	G3-C18	40.7 (6.4)
T4-A17	30.7 (6.1)	C4-G17	43.3 (5.7)
A5-T16	36.9 (5.7)	G5-C16	37.2 (6.5)
T6-A15	40.9 (5.0)	C6-G15	36.0 (5.1)
A7-T14	34.8 (2.9)	G7-C14	44.0 (10.1)
T8-A13	29.8 (3.8)	C8-C13	46.7 (5.7)
av	37.8 (5.1)		40.9 (4.2)
no. of base pairs/turn	9.5		8.8

[a] In degrees.

X and XI). The averaged helical repeat parameters and helical twist angles for the MP substituted AT and GC duplexes are most consistent with values reported for C DNA; a member of the B-DNA family (range 37–41, average 38.6°).[15,16] Similar helical repeat parameters are observed in both neutral DNA heteropolymers; however, the amount of helical unwinding is greatest for the neutral GC heteropolymer, at 8.8 base pairs per turn, which is slightly less than the average number of base pairs per turn in C DNA (9.0–9.3 pairs per turn).

Table XII. Predominant Sugar Conformational Populations over the 40-ps Molecular Dynamics Trajectory

AT			GC		
C2′ endo	T2-A19	C2′ endo	C2′ endo	C2-G19	C2′ endo
C2′ endo	A3-T18	C2′ endo	O1′ endo	G3-C18	C2′ endo
C2′ endo	T4-A17	C2′ endo	C2′ endo	C4-G17	C2′ endo
O1′ endo	A5-T16	O1′ endo	C2′ endo	G5-C16	O1′ endo
C2′ endo	T6-A15	C2′ endo	C2′ endo	C6-G15	C2′ endo
C2′ endo	A7-T14	C3′ endo	C2′ endo	G7-C14	O1′ endo
C2′ endo	T8-A13	C2′ endo	C2′ endo	C8-G13	C2′ endo
O1′ endo	A9-T12	O1′ endo	C2′ endo	G9-C12	C2′ endo

Table XIII. Conformational Subpopulations of DNA Sugars during Molecular Dynamics[a]

heteropolymer	C3′ endo, %	O1′ endo, %	C2′ endo, %
d[GCGCGCGCGC]$_2$	2	17	81
d[ATATATATAT]$_2$	12	25	63

[a] Values are shown as a percentage of the total furanose conformation in each heteropolymer during the 40-ps molecular dynamics trajectory.

Table XIV. Interstrand and Intrastrand Phosphorus Atom Distances (rms) for 40-ps Molecular Dynamics Trajectory

	intrastrand phosphorus distance, Å (rms)	
	GC	AT
overall	6.9 (0.2)	6.7 (0.2)
(*R*)-MP	6.7 (0.2)	6.6 (0.2)
(*S*)-MP	7.0 (0.2)	6.8 (0.2)
B DNA	7.0	
A DNA	5.9	
interstrand	17.4 (0.3)	17.3 (0.4)

The average furanose conformations (in Table XII) of the AT and GC duplexes from the molecular dynamics trajectories are consistent with B-type DNA conformations.[17,18] The predominant sugar conformation in both DNA systems over the dynamics trajectory is C2′ endo. The analysis of sugar subpopulations, shown as percentages of the total population for the entire trajectory, is given in Table XIII. An increase in the percentage of C3′ endo (A DNA) and O1′ endo sugar subpopulations is observed in the AT helix over the GC dsDNA. No difference between pyrimidine and purine furanose conformations was observed in either DNA helix.

The average intrastrand and interstrand phosphorous atom distances are shown in Table XIV. The intrastrand phosphorous atom distances are consistent with values observed in B-DNA-type structures.[18] The averaged (*S*)-MP intrastrand phosphorous atom distances are slightly greater than for (*R*)-MP in a consistent pattern. The GC intrastrand phosphorous distances are uniformly larger, albeit a small degree, than those observed in the neutral AT helix.

The majority of the backbone and glycosidic torsional angles of the neutral AT and GC helices (Table XV) were similar to values reported for B DNA (summarized from ref 18), with some notable variations. The average α dihedral angles of both DNA systems were consistent with an A-DNA conformation. The β

(15) Marvin, D. A.; Spencer, M.; Wilkins, M. H. F.; Hamilton, L. D. *J. Mol. Biol.* **1961**, *3*, 547–565.
(16) Leslie, A. G. W.; Arnott, S.; Chandrasekaran, R.; Ratliff, R. L. *J. Mol. Biol.* **1980**, *143*, 49–72.
(17) Westof, E.; Sundaralingam, M. *J. Am. Chem. Soc.* **1983**, *105*, 970–980.
(18) Saenger, W. *Principles of Nucleic Acid Structure*; Springer-Verlag: New York, 1984.

Table XV. Backbone and Glycosidic Torsion Angles (deg)

	α	β	γ	δ	ε	ζ	χ
	O3′–P′–O5′C	O5′C5′–C4′–C3	O5′–C5′–C4′–C3	C5′–C4′–C3′P	C4′–C3′–O3–P	C3′–O3′–P–O5′	Pur O1′–C1′–N9–C4 Pyr O1′–C1′–N1–C2
Ade	269.3 (17.1)	(*R*)-MP 174.2 (15.3)	85.3 (17.2)	122.2 (15.7)	222.3 (14.9)	234.7 (14.7)	231.5 (14.1)
Thy	277.7 (14.6)	(*S*)-MP 134.1 (15.3)	74.7 (11.8)	116.7 (14.5)	223.8 (10.4)	238.8 (12.4)	238.1 (14.1)
Gua	283.0 (11.5)	(*R*)-MP 168.9 (8.9)	58.7 (9.6)	131.2 (14.0)	224.5 (1.7)	224.0 (15.2)	247.6 (13.9)
Cyt	280.5 (14.7)	(*S*)-MP 140.6 (16.9)	64.3 (8.2)	126.1 (12.7)	223.2 (14.4)	223.7 (14.4)	241.8 (13.5)
A DNA	270	211	47	83	185	315	206
A DNA	285	181	59	79	205	293	202
B DNA	314	214	36	157	155	264	262
B DNA	299	180	57	122	173	269	241
B DNA	319	136	38	139	227	203	258
C DNA	321	200	37	157	161	254	263
C DNA	315	143	48	141	211	212	
D DNA	298	208	69	157	141	259	263
D DNA	287	223	89	146	136	275	250

Table XVI. Average Complementary Base-Pair Watson–Crick Hydrogen Bond Distances for the 40-ps Molecular Dynamics Trajectory

hydrogen bond	av length, Å (rms)
Gua O6-Cyt HN4A	2.06 (0.21)
Gua H1-Cyt N1	2.13 (0.11)
Gua HN2A-Cyt O4	2.05 (0.15)
Ade HN6A-Thy O4	2.23 (0.37)
Ade N1-Thy H3	1.96 (0.15)

dihedral averages were consistent with a B-DNA conformation in both systems, although the (*S*)-MP dihedral angles had significantly smaller values (>20° difference) compared to the (*R*)-MP β dihedral which are in the reported ranges for B- and C-DNA-type conformations. The γ dihedral values in both DNA systems are most consistent with those reported for D DNA, with the exception of guanine, which is more consistent with dihedral values reported for A- and B-type DNA conformations. The δ, ε, and χ dihedral values are in the B-DNA range. The averaged ζ dihedral values in both DNA heteropolymers are most consistent with a C-DNA conformation.

The average number of waters hydrogen bonded to the phosphate oxygen and base-pair hydrogen bond distances were examined carefully (Table XVI). Water hydrogen bonded to the sp^2 phosphoryl oxygen was determined by the presence of a hydrophilic atom (X) to oxygen atom distance of <3.5 Å, and an X–O bisector angle between 0° and 80°. The number of hydrogen-bonded waters coordinated to the phosphonate sp^2 oxygen averaged 2.2 waters per MP residue for the AT and GC helix. This is a significant decrease in the solvation of the phosphodiester backbone from native DNA, since there are approximately three hydrogen-bonded waters associated with each anionic phosphoryl oxygen (total of 6 waters per phosphate group) in native DNA.[7,19] The hydrogen bonds of the Watson–Crick paired bases remained intact throughout the simulation in both DNA systems. The hydrogen bond distances of both helical systems are foreshortened in comparison to unsubstituted phosphate DNA systems studied by molecular dynamics.[7,19,20] The average distances for the bases pairing are consistent with standard hydrogen bond distances NH···O = 1.95 Å and NH···N = 1.99 Å reported for X-ray crystal structures.[18]

Electrostatic Potential Surface Studies. The time-averaged DNA conformations and electrostatic potential surfaces of AT and GC helices during the 40-ps trajectory are shown in Figure 1. The neutral character of the electrostatic potential surface of the MP backbone at the solvent interface is clearly observed. The greater unwinding of the neutral GC dsDNA helix relative to the AT helix is readily observed, noting the foreshortening of the long axis and increase in diameter of the GC double helix. The electrostatic potential surfaces of the two neutral DNA systems have important differences. The electrostatic potential surface of the AT helix is almost uniformly neutral (green) in the major and minor groove, while the major groove of the GC helix shows several regularly spaced regions of strong electronegativity (red) corresponding to the O6 and N7 atoms of guanine on the face of the major groove. The minor groove electrostatic potential surface of both DNA systems appears relatively neutral at the solvent interface.

Discussion

From these molecular dynamics simulations we observe that uniform MP substitution of the phosphate backbone in dsDNA heteropolymers does not result in large conformational changes in DNA. On the basis of these findings, we propose that the negative charge of the phosphodiester, linkage does not play a major role in modulating the conformation of DNA. Neutralization of the native phosphate backbone in dsDNA heteropolymers by MP substitution results in two major changes in the DNA molecule: (1) an increase in the hydrophobic character of the backbone and (2) a localized effect of charge neutralization of the phosphate backbone, which mimics some of the effects of high cation concentration on DNA. The increased hydrophobic character of the MP-substituted backbone mimics the effects of low relative humidity mediated by interactions between the backbone and the water. This is evident by the nearly 3-fold reduction in the number of water molecules associated with the anionic phosphoryl oxygens in native DNA from 6 waters to 2.2 waters associated with the MP sp^2-hybridized phosphoryl oxygen. The MP substitution locally mimics the effect of high cation concentration on native DNA by neutralizing the negative native phosphate charge, and this effect does not result in major conformational changes since it is limited to the backbone. Thus, it is reasonable to consider that high cation concentrations effect large conformational changes (e.g., B to Z) through interactions with other regions of the DNA molecule in addition to the phosphate backbone.

Complete substitution of native phosphate groups with MP in these dsDNA heteropolymers increases the hydrophobic character of the helix (from the methyl groups) and alters the local solvation of the phosphate backbone of the DNA in a manner analogous to a reduction in the relative humidity. These findings are further supported by the observation that the hydration of the phosphate groups in MP-substituted dsDNA is reduced by more than half compared to native dsDNA, and the DNA helix undergoes transition to a C conformation—a "distorted" member of the B-DNA family. Factors favoring C-DNA conformation include (1) low relative humidity (75%) and very high NaCl content and (2) a rich AT content (low GC content).[21-24] In some instances

(19) Seibel, G. L.; Singh, U. C.; Kollman, P. A. *Proc. Natl. Acad. Sci. U.S.A.* **1985**, *82*, 6537–6540.
(20) Singh, U. C.; Weiner, P. K.; Seibel, G.; Kollman, P. A. *Proc. Natl. Acad. Sci. U.S.A.* **1985**, *82*, 755–759.
(21) Brahms, J.; Pilet, J.; Lan, T. P.; Hill, L. R. *Proc. Nat. Acad. Sci. U.S.A.* **1973**, *70*, 3352–3355.
(22) Mahendrasingam, A.; Rhodes, N. J.; Goodwin, D. C.; Nave, C.; Pigram, W. J.; Fuller, W. *Nature* **1983**, *301*, 535–537.
(23) Rhodes, N. J.; Mahendrasingam, A.; Pigram, W. J.; Fuller, W.; Brahms, J.; Vergne, J.; Warren, R. A. J. *Nature* **1982**, *296*, 267–269.

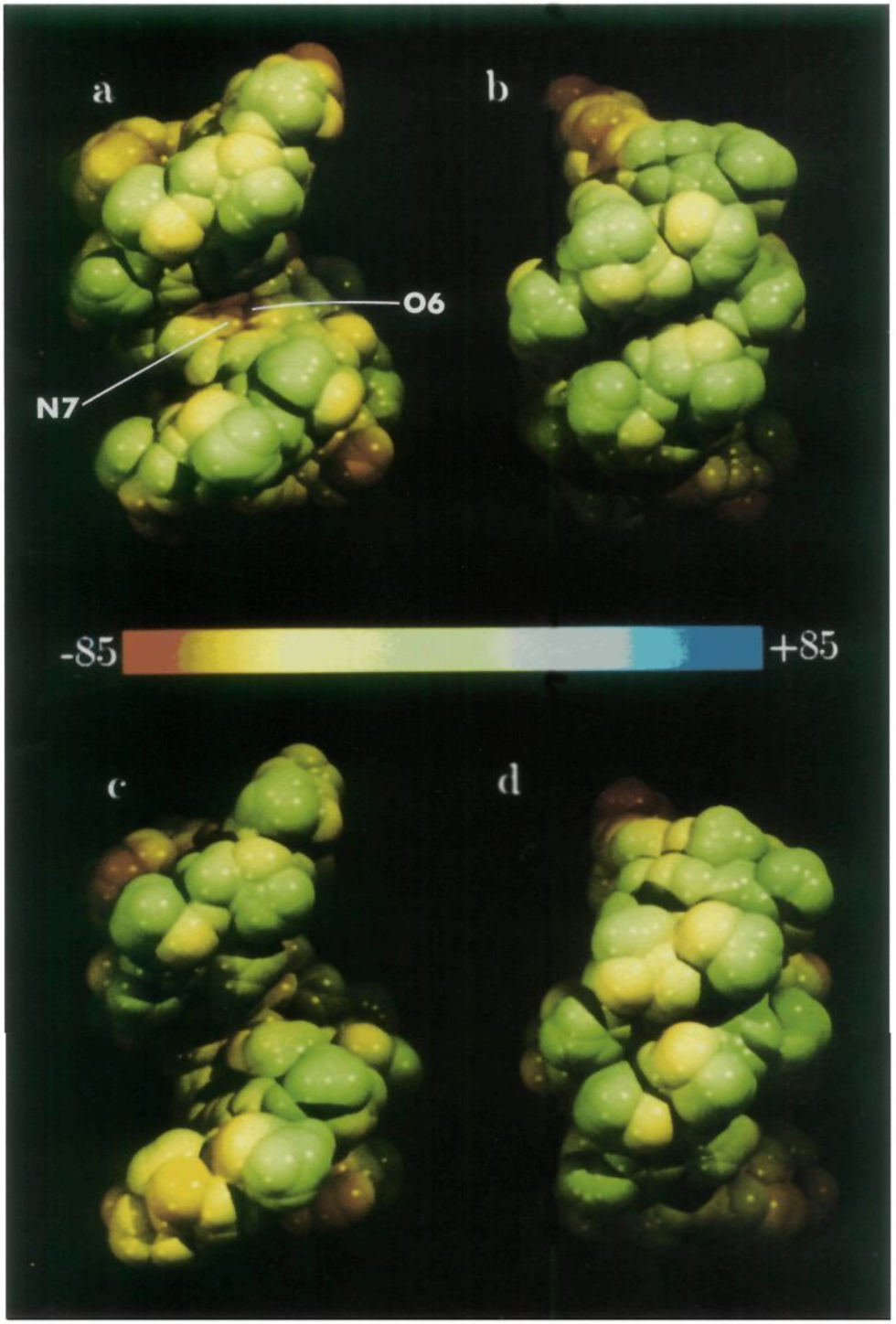

Figure 1. Electrostatic potential surface of methyl phosphonate dsDNA heteropolymers. Structures a and b are views into the major and minor grooves, respectively, of d[GC]5-d[GC]5, and c and d are major and minor groove views of d[AT]5-d[AT]5. Note the larger degree of helical unwinding and the more negative (red) electrostatic potential surface in the major groove centered on atoms O6 and N7 of guanine in the GC helix.

the C-DNA conformation is observed under conditions of high relative humidity (95%) and very low NaCl content.[21] In general, the conditions favoring the C conformation are intermediate between those favoring A- and B-DNA conformations, and the C to B conformational transition can be induced by increasing the relative humidity of the DNA.[9,16] Experimental characterization of the conformational transitions involving C DNA as a function of salt concentration and relative humidity support our findings. The electrostatic potential surface of neutral DNA shows that atom O6 of guanine is the most electronegative atom accessible to the solvent. The electrostatic potential surface of AT is uniformly neutral at the solvent interface. These observations are consistent with the lipophilic nature of the MP-substituted oligomers.

Increasing the hydrophobic character and neutralizing the negatively charged phosphate backbone of dsDNA by methyl substitution of one anionic phosphoryl oxygen in the phosphodiester

(24) Fuller, W.; Wilkins, M. H. F.; Wilson, H. R.; Hamilton, L. D. *J. Mol. Biol.* **1965**, *12*, 60–80.
(25) Arnott, S.; Chandrasekaran, R.; Hukins, D. W. L.; Smith, P. J. C.; Watts, L. *J. Mol. Biol.* **1974**, *88*, 523–533.

backbone results in a series of specific changes in the physicochemical behavior of solvated dsDNA heteropolymers. These effects include helical unwinding, a marked decrease in the solvation of the phosphate backbone, and conformational alterations in the backbone dihedral angles. To study these effects in a realistic manner, molecular dynamics simulations were carried out using periodic boundary conditions simulating the DNA in an infinite dilution of solvent. The major effect of charge neutralization of the native phosphate backbone by methyl substitution is to partially mimic the effect of high cation salt concentration and reduced solvation by inducing a C-DNA conformation. This effect is limited to the backbone, since these dsDNA molecules do not adopt a Z-DNA conformation, suggesting that high cationic salt concentration and interactions with other atoms (e.g., the bases and sugar groups) are essential for facilitating this conformational transition. It is known that single-strand MP DNA oligomers adopt a B-DNA conformation in solution.[2] It is possible that the MP modification could stabilize the Z-DNA conformation of certain DNA base sequences and special conditions, and this is an area we are presently investigating.

Studies of single-strand MP DNA oligomers have shown that the MP modification reduces the effect of salt concentration with regard to duplex hybridization and stabilization.[1] To our knowledge, studies of completely neutral (both DNA phosphate backbones substituted by MP) dsDNA molecules have not been reported previously. Our data suggest that MP substitutions in both DNA strands of similar heteropolymers will result in the formation of stable B-DNA-type (C-DNA) helices in water and have unique sequence-dependent conformational and electrostatic features at the DNA–solvent interface. Collectively, these findings are important in terms of understanding the role of the negative phosphate backbone in stabilizing native DNA and determining some of the physicochemical behavior and may be useful in the rational design of modified DNA oligomers containing other chemical substitutions of the native backbone. The role of the negative phosphate backbone in genetic replication, transcription, and translation is poorly characterized at present and has far-reaching implications for understanding many critical processes in biology and potentially novel diagnostic and therapeutic approaches. We believe that, with increased utilization of similar approaches and computer technology, improved progress can be made to enhance the understanding in areas such as chemical drug design.

Acknowledgment. All calculations were carried out on the CRAY X-MP/24 at the Center for High Performance Computing at the University of Texas System in Austin, TX, the National Cancer Institute, and the CRAY X-MP14/SE at Scripps. This research was supported by academic grants from Cray Research (K-GAHM-XX-531-2-99 and K-531-1-99) and by Federal funds from the Department of Health and Human Services under Contract N01-CO-74102 with Program Resources, Inc. The content of this publication does not necessarily reflect the views of policies of the Department of Health and Human Services, nor does mention of trade names, commercial products, or organizations imply endorsement by the U.S. Government.

Registry No. $d[GC]_{10}$ methyl phosphonate substituted, 130095-87-3; $d[AT]_{10}$ methyl phosphonate substituted, 130095-88-4; deoxyadenosine, 958-09-8; thymidine, 50-89-5; deoxyguanosine, 961-07-9; deoxycytidine, 951-77-9.